3rd EuCheMS Chemistry Congress

Sodium Effect on Self-Organization of Amphiphilic Carboxylates: Formation of Structured Micelles and Superlattices

Karin Rosenlehner,[a] Boris Schade,[b] Christoph Böttcher,*[b] Christof M. Jäger,[c, d] Timothy Clark,*[c, d] Frank W. Heinemann,[e] and Andreas Hirsch*[a, d]

Abstract: Not only the self-aggregation of dendritic polycarboxylates into structurally persistent micelles, but also that of the micelles themselves into superlattices is controlled by alkali-metal counterions and shows a pronounced sodium effect. Our combined experimental and computational work has revealed the formation of superlattices for the first time. The behavior of a variety of amphiphilic carboxylates and the different effects of the alkali cations Li^+, Na^+, and K^+ have been investigated by conductivity measurements, cryogenic transmission electron microscopy (cryo-TEM), and molecular-dynamics (MD) simulations. Together, these show that sodium salts of the amphiphiles give the most stable micelles, followed by lithium and potassium. Our results suggest that ion

Keywords: aggregation · amphiphiles · dendrimers · micelles · specific-ion effects

multiplets in bridging positions, rather than contact ion pairs, are responsible for the enhanced stability and the formation of hexagonally ordered superlattices with sodium counterions. Potassium ions do not form such ion multiplets and cannot therefore induce aggregation of the micelles. This sodium effect has far-reaching consequences for a large number of biological and technical systems and sheds new light on the origin of specific-ion effects.

Introduction

The supramolecular aggregation of amphiphiles in aqueous media was one of the key processes that led to the development of life on earth. The most striking example is the formation of cell membranes by lipid molecules. However, an analogous self-organization process also leads to structurally persistent micelles,[1–4] that is, absolutely monodisperse soft nanoparticles. Self-organization that leads to absolutely reproducible nanoparticles (in size and shape) is remarkably

[a] Dr. K. Rosenlehner, Prof. A. Hirsch
Department of Chemistry and Pharmacy
Interdisciplinary Center of Molecular Materials (ICMM)
Friedrich-Alexander-Universität Erlangen-Nürnberg
Henkestrasse 42, 91054 Erlangen (Germany)
Fax: (+49) 9131-852-6864
E-mail: andreas.hirsch@chemie.uni-erlangen.de

[b] Dr. B. Schade, Dr. C. Böttcher
Research Center for Electron Microscopy
Department of Chemistry and Biochemistry
Freie Universität Berlin, Fabeckstrasse 36a, 14195 Berlin (Germany)
Fax: (+49) 30-838-56589
E-mail: bottcher@chemie.fu-berlin.de

[c] Dr. C. M. Jäger, Prof. T. Clark
Computer-Chemie-Centrum and
Interdisciplinary Center for Molecular Materials
Department of Chemistry and Pharmacy
Friedrich-Alexander-Universität Erlangen-Nürnberg
Nägelsbachstrasse 25, 91052 Erlangen (Germany)
Fax: (+49) 9131-852-6565
E-mail: tim.clark@chemie.uni-erlangen.de

[d] Dr. C. M. Jäger, Prof. T. Clark, Prof. A. Hirsch
Excellence Cluster "Engineering of Advanced Materials"
Friedrich-Alexander-Universität Erlangen-Nürnberg
Nägelsbachstrasse 49b, 91052 Erlangen (Germany)

[e] F. W. Heinemann
Department of Chemistry and Pharmacy
Friedrich-Alexander-Universität Erlangen-Nürnberg
Egerlandstrasse 1, 91058 Erlangen (Germany)
Fax: (+49) 9131-852-7367

Supporting information for this article is available on the WWW under http://dx.doi.org/10.1002/chem.201001150.

rare and of immense importance for future nanotechnologies. It is therefore essential that we can understand the factors that influence the size, shape, and behavior of structurally persistent micelles.

The spontaneous self-organization of micelles is generally thought to be due to entropy-controlled hydrophobic interactions, which also play an important role in the early stages of protein folding. It has long been known that ions affect protein solubility, as originally described in the Hofmeister series.[5–7] Earlier interpretations of these effects classed ions as "water structure makers", which are strongly hydrated and have stabilizing and salting-out effects on proteins, and "water structure breakers", which destabilize folded proteins in solution and can even denature them. Hofmeister's work still enjoys considerable interest as it is relevant to a broad range of fields, such as enzyme activity,[7–9] protein stability,[10] or protein–protein interactions.[11,12] Another eminent example for the pronounced influence of ions in biological processes is the Na–K pump in living cells, whereby Ca^{2+} and Na^+ ions are pumped out of living cells, whereas K^+ is pumped in. This is because Ca^{2+} and Na^+ are well matched to the major intracellular anions like phosphates, carboxylates, and carbonates and tend to form contact ions with these species. K^+, in contrast, stays away from the major intracellular anions, increasing the net charge and thus solubility of molecules containing these anionic groups and also leaving these anionic groups available to act as binding determinants.[13]
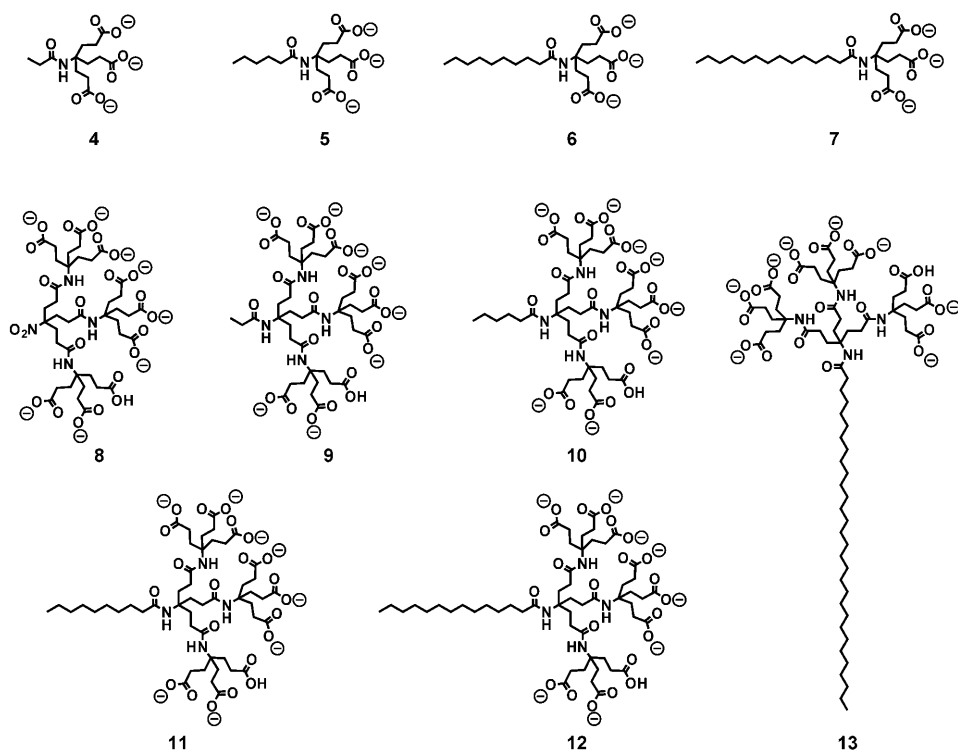
Recent theoretical studies on biological systems such as membranes, nucleic acids, and surfaces of proteins support the theory that interactions with ions present in the aqueous environment play a fundamental role for aggregation and stability.[14,15] The importance of the nature of the counterion for the aggregation of amphiphiles has been overlooked so far. However, despite the obvious importance of the specific-ion effects for macromolecules in aqueous solution, the mechanisms of ion interaction at an atomic level are still not clear.[16]

We have recently developed several new families of amphiphiles, which are uniquely suitable models for investigating aggregation processes in water systematically.[17] These amphiphiles all feature a rigid functionalizable conjugated π system—such as a calixarene, a fullerene, or a perylene—as the central platform (see formulae 1–3). These platforms allow a variety of hydrophilic and hydrophobic head and tail groups to be bound in a stereochemically controlled and tunable fashion. As polar heads we have mainly used Newkome-type oligo-carboxylic acids, which at neutral pH values are predominantly deprotonated and guarantee excellent water solubility. Compounds 1 and 3 exhibit unprecedented properties, such as the formation of shape-persistent micelles, whose defined structure has been resolved at the molecular level.[1–3,18] Amphiphilic perylenes such as 2[19,20] show a very pronounced and selective exfoliation efficiency for the dissolution, individualization, and doping of carbon nanotubes[21–23] and graphene.[24]
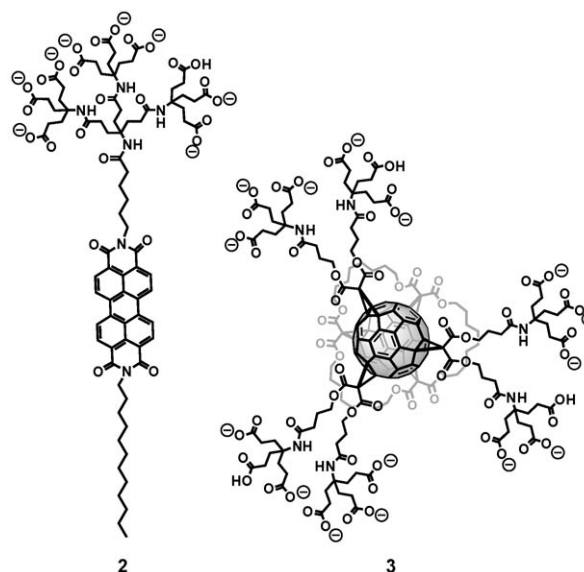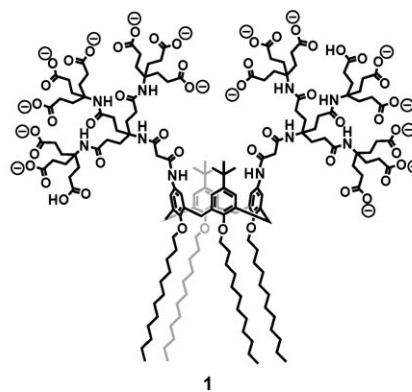
Our recent work on the formation of shape-persistent micelles has shown that not only the structure of the amphiphiles themselves, but also the nature of the counterions of the polycarboxylate termini determines the stability and structure of the micelles. Molecular dynamics (MD) simulations and cryogenic transmission electron microscopy (cryo-TEM) experiments have revealed that the micelles are specifically stabilized by sodium relative to potassium counterions. These studies suggest that the micelles are stabilized by strongly conserved hydrated contact ion pairs[25] and especially $RCO_2^-\cdots M^+\cdots RCO_2^-$ ion triplets that consist of two carboxylates and one counterion with sodium but not with potassium ions. We now report a significant breakthrough, both in our understanding of the factors that control the size and shape of the micelles and in making use of the specific-ion effect to introduce a further level of self-organization to obtain regular arrays of structured micelles.

For this purpose, we have synthesized a series of new single-tailed Newkome-type dendritic surfactants 4–13, which lack a rigid aromatic platform and thus represent minimal models of the amphiphiles shown above. We now show that the presence of sodium as counterion leads not only to a considerable stabilization of the micelles them-

over and above that represented by the micelles themselves. Thus, this investigation not only represents considerable progress towards the rational design of hierarchically ordered mesophases and nanomaterials, but also towards the understanding of assembly and folding principles of monodisperse synthetic and biological aggregates.

Results and Discussion

Synthesis of the single-tailed amphiphiles **4–13** was accomplished by either esterification with acyl chloride or Steglich esterification of the lipophilic chain building block with the first- or second-generation Newkome dendrimers **14** or **19**.[26–28] The dendrimer provides a bulky head group and serves as the hydrophilic part after acidic deprotection of the *tert*-butyl esters. Scheme 1 shows the reaction cascade towards the target molecules. All compounds were fully characterized by NMR spectroscopy, MS, IR spectroscopy, and elemental analysis.

selves relative to lithium and potassium, but also induces very specific micelle–micelle interactions that lead to highly ordered superlattices. These structures represent a further important step in the controlled self-organization of soft particles as they provide an additional level of organization
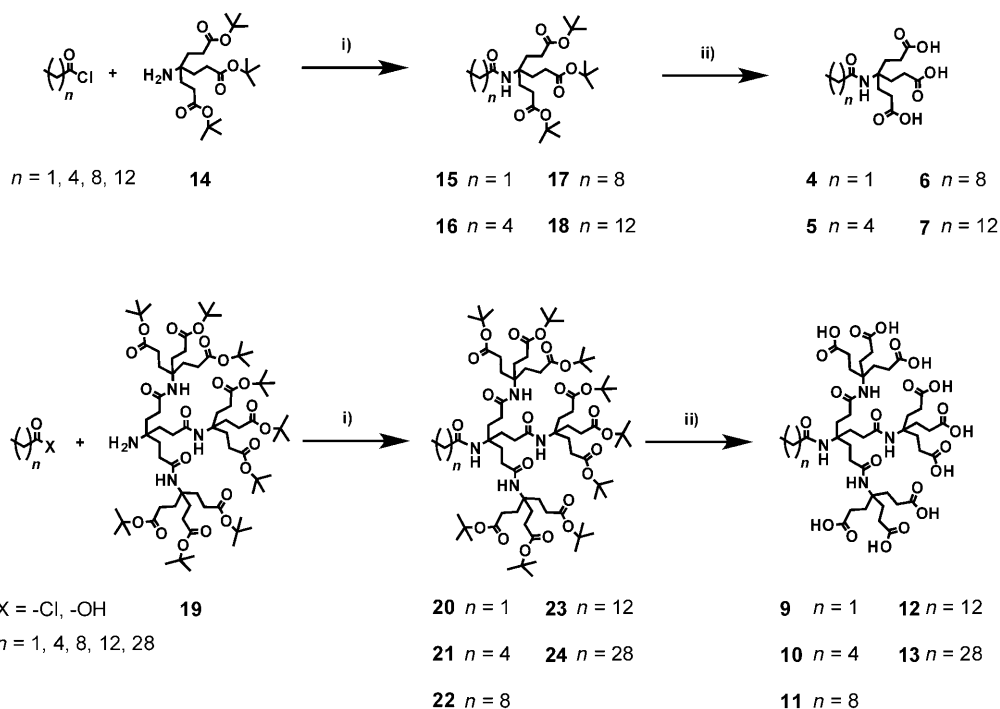
Scheme 1. Synthesis of compounds: i) Et₃N, CH₂Cl₂, hydroxybenzotriazole (HOBt), DMF, RT for X = Cl or *N,N*-dicyclohexylcarbodiimide (DCC), 0 °C for X = OH; ii) HCOOH, RT.

Recrystallization of amphiphile **6** from water led to the formation of single crystals suitable for X-ray analysis (for details see the Supporting Information). Bond lengths and angles of the molecular structure of **6** do not show anomalies (Figure 1) . The central carbon atom C2 features the typical tetrahedral configuration with only slight deviations of the angles from the ideal value of 109.5°. The alkyl chain is arranged in an all-*trans* fashion.
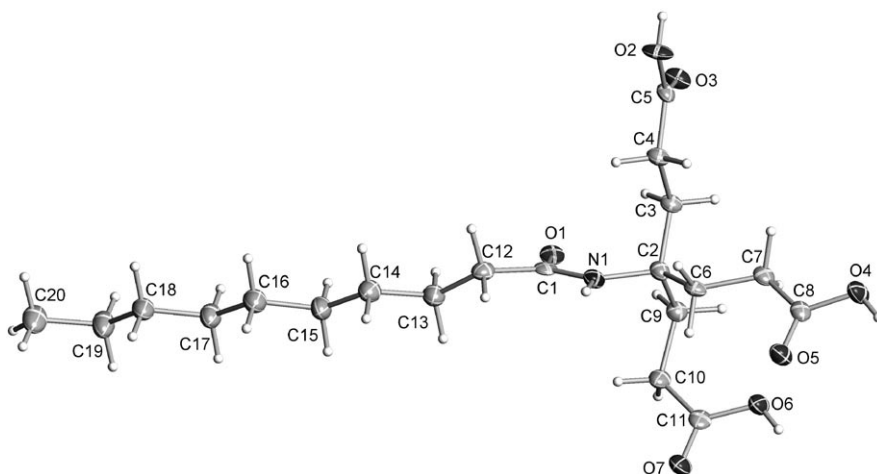

Figure 1. Molecular structure of compound **6** (50 % probability ellipsoids, hydrogen atoms were drawn at an arbitrary size).

The packing is characterized by efficient use of van der Waals interactions between the apolar alkyl chains and by hydrogen bonding of the carboxyl groups. In particular, dimers are built up by hydrogen bonding between two acid groups of the dendrimer. The third dendritic arm forms a hydrogen bond to the carbonyl group of the amide moiety of an adjacent molecule (Figure 2). In the parallel-oriented chains, all C atoms are separated by a distance of 5.5 Å,
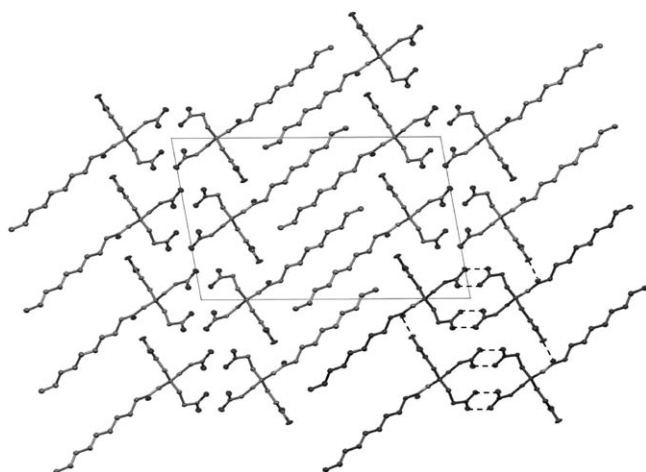

Figure 2. Packing diagram of compound **6**; view along the crystallographic *b* axis highlighting the parallel arrangement of the alkyl chains and the hydrogen bridging situation.

while the distance between C atoms of the antiparallel intercalated chains is only about 4.1 Å.

Investigation of micelle stability through conductivity measurements: One of the most important parameters that describe the stability of micelles is the critical micelle concentration (cmc), the lowest concentration at which micelles form.[29] Physical properties like viscosity, density, and surface tension of solutions undergo distinct changes at the cmc,[30] and the specific conductivity (κ) changes dramatically when the cmc is reached. At concentrations below the cmc, the monomeric oligoelectrolyte contributes linearly as a multiply charged ion to the conductivity of the solution with increasing concentration. As the aggregates formed at and above the cmc are larger and less mobile than the monomer, each monomer now contributes less to the overall conductivity. In this context we focused on the investigation of the aggregation of amphiphiles **8**–**13**, which contain the corresponding second-generation dendrons. Figure 3 shows a typical diagram of specific conductivity (κ) versus the concentration of amphiphile. The intersection of the two straight lines indicates the change of properties and was defined as the critical micelle concentration.
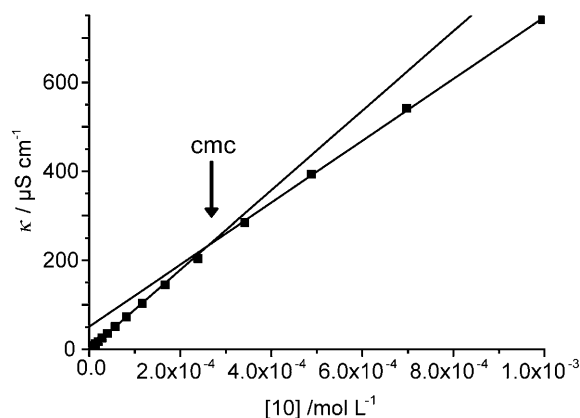
Figure 3. Specific conductivity versus concentration of compound **10** as a sodium salt. At the critical micelle concentration the conductivity changes dramatically as aggregates contribute less to the overall conductivity as monomers. The intersection of both lines is defined as the cmc.

As counterion binding plays an important role in determining aggregation, all measurements were carried out in a pure aqueous solution, rather than buffer solutions. The am-

phiphiles were titrated with nine equivalents of NaOH, KOH, or LiOH to obtain the corresponding salts that provide the desirable water solubility. Varying the counterions now allows for the investigation of the influence of alkali-metal ions on the aggregation strength of the surfactants by comparing the different cmc values. The results are summarized in Table 1.

Table 1. Overview of the critical micelle concentrations (cmc's) of lithium, sodium, and potassium salts of compounds **8–13**.

Compound	cmc Li salt [mol L^{-1}] × 10^{-4}	cmc Na salt [mol L^{-1}] × 10^{-4}	cmc K salt [mol L^{-1}] × 10^{-4}
8	4.26	4.00	4.71
9	3.53	2.88	3.94
10	3.08	2.60	3.47
11	2.68	2.00	3.54
12	2.32	1.80	3.38
13	2.16	1.39	3.22

Figure 4 shows a plot of the cmc values against the chain length, which reveals an exponential decrease of the cmc with increasing chain length. Longer alkyl chains stabilize the aggregates up to a certain chain length.
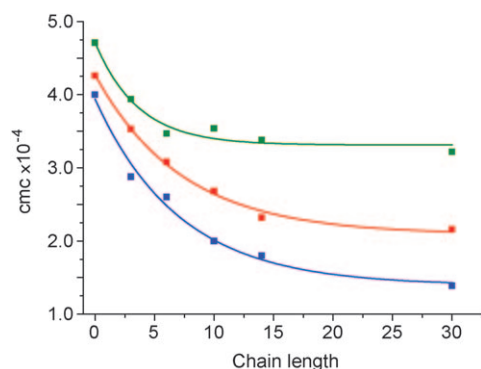

Figure 4. Plot of cmc versus chain length of compound **8–13** as sodium (blue), lithium (red), or potassium (green) salts.

Further lengthening of the hydrophobic chain causes no additional stability of the micelles. However, not only the chain length influences the cmc, but also the nature of the counterion. The most stable micelles are formed if sodium is used as the counterion, followed by lithium. Samples with potassium as the counterion are found to form relatively instable micelles (Figure 4). We also performed additional pulsed-gradient spin-echo (PGSE) NMR spectroscopy experiments, which showed that the particle size increases with increasing chain length. This effect is ascribed to the enhanced steric demand of longer chains (see the Supporting Information).

Cryo-TEM measurements: Cryo-TEM has proven to be an excellent technique for visualizing physically associated microstructures. Rapid thermal quenching leaves the amphi-

philic assembly unperturbed and results in a high-quality image of the aggregate in its habit in solution.[31] We investigated compound **13** in water during addition of NaOH and KOH. At pH 5–6, both solutions were found to contain fiberlike micelles with diameters of 73 Å (Figure 5a and b). Spherical micelles of diameter 76 Å were also found in the sodium sample, but not in the potassium sample (Figure 5c).

At pH 6.4, both samples show exclusively spherical micelles of diameter 67 Å (Figure 5d and e). However, we also observe a remarkable intermicelle aggregation effect. In contrast to the corresponding potassium salts, the sodium
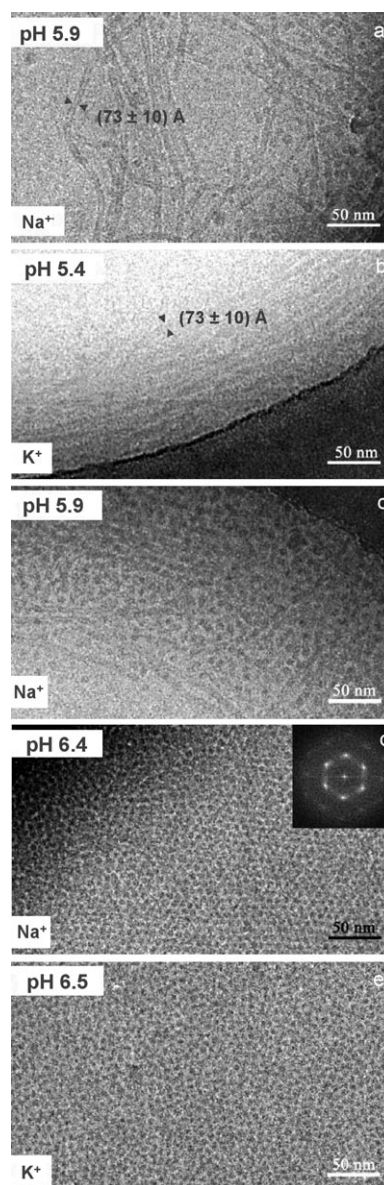
Figure 5. Cryo-TEM images of compound **13** as sodium (a,c,d) and potassium (b,e) salts at different low-pH values. The aggregate diameter of the obtained fibrils is quite similar, but the sodium salt forms additional spherical micelles (c). At pH 6.4 the sodium salt (d) forms ordered (mono)layers of densely packed spherical micelles. FFT (inset) of the image shows sharp hexagonal reflexes (d) reflecting the high degree of ordered micelle packing.

micelles form highly ordered (mono)layers of densely packed micelles. Fast Fourier transform (FFT) of such highly ordered areas shows sharp hexagonal reflexes at (69 ± 1) Å and less sharp reflexes of higher order, as shown in Figure 5d in the inset.

The investigations were emphasized by TEM measurements of sodium phosphate buffered solutions and 1% phosphotungstic acid (PTA) as contrast medium. At low pH (pH 4.3) only fiberlike micelles occur with a very consistent diameter of 65 Å (Figure 6a). At pH 5.7 spherical micelles
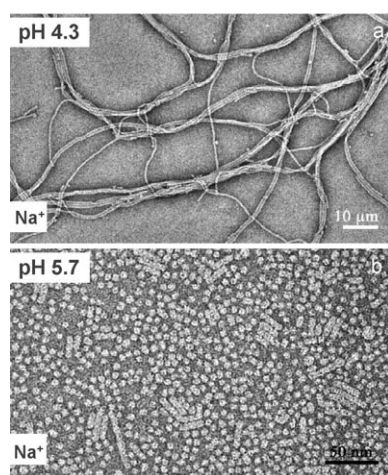

Figure 6. TEM image of compound **13** in sodium phosphate buffer, contrasted with 1% PTA. a) At low pH only fiberlike micelles occur with a very consistent diameter of 65 Å. b) At pH 5.7, spherical micelles with atypical, very distinct edges can be detected.

can be detected. These micelles possess atypical, very distinct edges (Figure 6b). The fact that the sizes of micelles at certain pH do not exactly match those of the pure salt can be ascribed to preparation influences in the contrasted samples. The change of pH causes the appearance of spherical micelles already at pH 5.7, and not at pH 6.4 as it is in non-contrasted samples. Significant is the establishment of highly ordered packing motifs (Figure 6b), which also suggests the presence of efficient intermicellar interactions promoted by the sodium counterions.

The sodium salt aggregates of the micelles in all the cryo-TEM images show high contrast with sodium counterions. Our earlier work suggests that this is because of high-density hydrated contact ion pairs with sodium counterions.[32] Hydrated sodium carboxylate contact ion pairs and multiplets are more dense than water, whereas fully hydrated potassium ions are less dense.[32] High local concentration of solvated sodium contact ion multiplets on the micelle surface leads to a higher density and enhanced contrast, which can easily be monitored by cryo-TEM without the addition of staining salts.

In addition to the conductivity measurements, these cryo-TEM investigations emphasize the dominant influence of counterions on the formation of aggregates and micelles. One possible explanation is that according to the Hofmeis-

ter series, Li$^+$ and Na$^+$ ions and carboxylates are strongly hydrated in comparison with K$^+$ ions.[33] Collins and co-workers have proposed the "law of matching water affinities", which suggests that oppositely charged ions with equal water affinities tend to form contact ion pairs in solution, whereas those with different water affinities tend to form solvent-separated ion pairs.[33,34] Another possible explanation is that the chelate effect of carboxylates is important for their binding to cations.[35] The lithium ion is thought to be too small to match the two-point binding of carboxylates and the potassium ion too big, whereas Na$^+$ fits perfectly.[36] However, neither of these explanations provide a rationalization of the results at the atomistic level. To answer these questions we have performed molecular dynamics (MD) simulations to help us to understand the effects reported above and those found in our earlier work.[25,32]

MD simulations: The results described above allow us to understand many of the factors that lead to the observed specific-ion effects. We previously attributed the ion-specific stabilization of the micelles by sodium relative to potassium to a reduction of the electrostatic repulsion of the head groups through electrostatic shielding provided by the closely associated sodium ions.[32] Sodium ions were found to be strongly conserved in bridging positions between carboxylates or between carboxylate and amide carbonyl groups of the dendrimer. This bridging stabilizes the micelles and also allows the head groups to adopt staggered conformations that are crucial for the formation of small micelles with high curvature.[25] In contrast, the lower electrostatic shielding and absence of specific bridging contacts with potassium ions leads to higher repulsion between the head groups that is compensated by a larger hydrophobic core and lower curvature of the aggregate.[32] These effects may also explain why only fiberlike micelles and no spherical micelles are formed at low pH in potassium salt solutions (Figure 5).

This effect can also explain the pH dependence of micelle formation; the formation of strongly conserved hydrated contact ion triplets paradoxically reduces the electrostatic repulsion when more carboxylic acid groups are deprotonated because strong specific intercarboxylate bridging by sodium ions replaces weaker hydrogen bonds.

Recently, Hess and van der Vegt investigated cation-specific binding with charged residues on proteins using molecular dynamics simulations.[37] In addition to biomolecular systems they also performed simulations on lithium, sodium, and potassium acetate solutions. They observed significant differences between free acetate in solution and surface-embedded carboxylates. They emphasized the preference for so-called "solvent-shared" ion pairs over the formation of stable contact ion pairs (CIPs) for the acetate solutions, rather than for the embedded carboxylates.

We therefore performed "dimer" simulations in which two Newkome-type dendritic head groups were initially placed "head to head" (i.e., with their polycarboxylate groups facing each other) in a water box large enough to allow dissociation to investigate intermicelle binding with

molecular dynamics. The monomeric dendrimer amphiphiles **1** was chosen for the simulations. Our rationale was that previous experience[25,32] suggests that dissociation of even carefully pre-equilibrated oligomeric structures that are inherently unstable is fast on our MD timescale. Thus, the purpose of our simulations was to detect fast dissociation of such inherently unstable aggregates. The protocol used to carry out the MD simulations is given in the Supporting Information. Figure 7 shows plots of the mean values of the shortest intermonomer O–O distances for all carboxylate oxygen atoms as a function of the simulation time for the lithium, sodium, and potassium salts of the dendrimers.
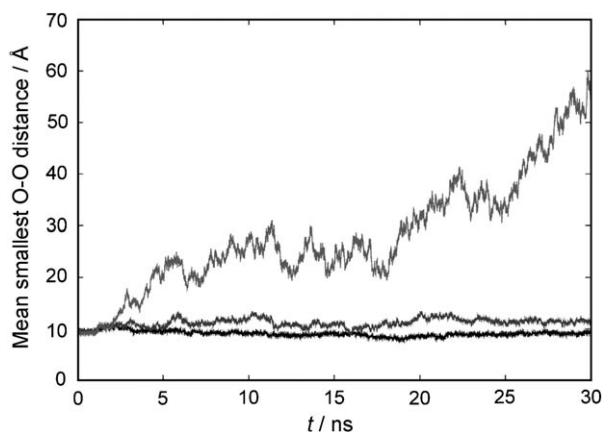

Figure 7. Plot of the mean smallest O–O distance between monomers of **1** for the simulations with lithium (top), sodium (middle), and potassium (bottom) counterions. Each simulation contains a total of 65 metal cations and 29 chloride ions. A detailed analysis of the smallest O–O distances demonstrating the evolution of interactions between the carboxylates is given in the Supporting Information.

The plots clearly show that the "dimer" of the potassium salt dissociates within 10 ns, whereas those of the lithium and sodium salts remain stable over the entire length of the simulation. The mean smallest O–O distances over the trajectories after 10 ns are 9.4 and 11.1 Å for the lithium and sodium salts, respectively, whereas the potassium salt dissociated to a distance of more than 30 Å after 20 ns simulation. The intermonomer distance for the lithium simulation is also very stable, which suggests a much more rigid dimerization surface than that for sodium.

The data show, as expected, that lithium and sodium have a far higher propensity to form contact ion pairs than potassium (Table 2). Note that single ion pairs can either be formed by monodentate or bidentate binding of the cation to the carboxylate. Thus, they contribute differently to the sum of contacts. However, the two smaller ions also form significant numbers of ion triplets (ITs). In these ion triplets two carboxylate anions are bridged by one cation in contrast to contact ion pairs (CIP) in which the carboxylate and cation build a one-to-one complex. Quite generally, the number of cation–anion contacts decreases with increasing size of the metal ion, but the ratio between the number of

Table 2. Distribution of ion pairs (CIPs), cation-bridged ion triplets (ITs), and the sum of all cation–anion contacts together with the IT/CIP ratio of **1** from the simulations. The IT/CIP ratio is highest for simulations with sodium counterions. Details of the simulations and analysis are given in the Supporting Information.

Metal ion	Sampling period [ns]	Average number of each species			IT/CIP
		CIP	IT	Total[a]	
Li	0–5	29.3	9.8	79.2	0.33
	5–10	25.9	11.9	82.1	0.46
	10–15	23.3	14.0	84.5	0.60
	15–20	23.0	13.9	85.3	0.61
	20–25	24.6	12.6	85.0	0.51
	25–30	22.7	13.3	84.6	0.59
Na	0–5	16.6	10.4	57.5	0.63
	5–10	11.0	6.3	36.2	0.57
	10–15	8.9	4.0	27.5	0.46
	15–20	6.9	7.3	35.3	1.07
	20–25	7.0	11.4	50.4	1.62
	25–30	7.2	9.8	44.5	1.35
K	0–5	9.4	4.6	26.3	0.48
	5–10	7.5	1.3	14.3	0.17
	10–15	6.8	1.9	14.4	0.27
	15–20	6.4	2.7	16.1	0.42
	20–25	7.4	1.6	14.7	0.22
	25–30	6.5	1.9	13.8	0.29

[a] Total cation–anion contacts.

contact ion pairs and the number of ion triplets is highest for sodium. The simulations indicate that the number of contact ion triplets is important for aggregation, which suggests that simple contact ion pairs are not sufficient to induce aggregation. The fact that sodium forms proportionally more contact ion triplets than lithium (i.e., the IT/CIP ratio is higher, see Table 2) may also be the reason that it has the lowest cmc of the three metals. The balance between the interaction energies of the metal ion with water and carboxylate anions (both of which decrease in the order Li > Na > K) and the strong hydrogen bonds between coordinated carboxylates and water molecules of the second solvation sphere[32] are both important. We will present a quantitative analysis of these effects based on density functional theory calculations on hydrated ions, ion pairs, and ion triplets. The results of the current simulations are analyzed in more detail in the Supporting Information.

Conclusion

Our work reveals that sodium salts of amphiphilic carboxylates give the most stable aggregates, followed by the lithium and potassium salts. Strongly bound contact ion multiplets allow sodium salts to form spherical micelles at low pH, whereas potassium derivatives only form fiberlike aggregates under the same conditions. At higher pH, the sodium amphiphiles form highly ordered monolayers with densely packed, hexagonally ordered micelles. MD simulations show that, whereas lithium forms the highest concentration of contact ion pairs in aqueous solutions of carboxylate salts,

sodium prefers to form bridging $RCO_2^-\cdots Na^+\cdots RCO_2^-$ ion triplets. Moreover, the simulations suggest that the number of contact ion multiplets, rather than simple contact ion pairs, is important for aggregation. If we assume that contact ion pairs stabilize monomers slightly better than micelles, but ion triplets stabilize the latter preferentially because of additional intermonomer contacts, the relative abundance of ion triplets for the sodium salt should lower the cmc. Specific-ion effects in biological systems (protein aggregation and polymerization, protein stability, or protein–DNA interactions) are fundamental for both their structure formation and function. Our findings reveal the important role of ion triplets and multiplets for the interaction of surface-embedded polycarboxylates and highlight the unique role of sodium counterions. Note once more that these effects are considerably less strong for free acetates in solution than for polycarboxylates. We hardly need to emphasize that these findings have far-reaching consequences for all biological and technical systems that involve polyanions in aqueous solution. Thus, 120 years after Franz Hofmeister's work, specific-ion effects still harbor surprises.

Experimental Section

All chemicals were purchased from Sigma–Aldrich and Acros Organics. The products were purified by flash chromatography on silica gel 60M (grain size 0.04–0.063 nm, less active) from Macherey–Nagel. ^{1}H and ^{13}C spectra were recorded with Bruker Avance 300, JEOL JNM EX 400, JEOL JNM GX 400, and JEOL A 400 spectrometers. Solvent peaks were used as references. Resonance multiplicities are referred to as s (singlet), d (doublet), t (triplet), and m (multiplet). Mass spectra were measured by Micromass Lab Spec (FAB) with 3-nitrobenzyl alcohol (NBA) as the matrix. MALDI-TOF mass spectra were acquired on an AXIMA-CFR plus instrument (Kratos Analytical, Manchester, UK) with 2,5-dihydroxybenzoic acid (DHB) as the matrix. Elemental analyses were performed with an EA 1110 CHNS analyzer (CE instruments). Conductivity was measured with a Cond 340i hand-held conductivity meter from WTW.

Cryo-TEM measurements

Samples: All samples were prepared as 1.25 mM solutions in water. The desired pH was adjusted by careful titration with 0.1 M sodium hydroxide or potassium hydroxide, respectively.

Sample preparation for cryo-TEM: Droplets of the corresponding sample solution (5 μL) were applied to perforated (1 μm hole diameter) carbon-film-covered 200 mesh grids (R1/4 batch of Quantifoil Micro Tools GmbH, Jena, Germany). The carbon layer had been hydrophilized prior to use by 60 s plasma treatment at 8 W in a BALTEC MED 020 device. The supernatant fluid was removed with a piece of filter paper until an ultra-thin layer (100–200 nm) was obtained spanning the holes of the carbon film. The samples were subsequently vitrified by propelling the grids into liquid ethane at its freezing point (90 K) by operating a guillotine-like plunging device. Ultra-fast cooling is necessary for an artifact-free thermal fixation (vitrification) of the aqueous solution avoiding crystallization of the solvent or rearrangement of the assemblies.

Cryo-TEM: The vitrified samples (see above) were transferred into a Philips CM12 transmission electron microscope (FEI Company, Oregon, USA) using the Gatan (Gatan Inc., California, USA) cryo-holder and -stage (Model 626) while cooling with liquid nitrogen. Microscopy was carried out at a sample temperature of 94 K using the low-dose protocol of the microscope at a primary magnification of $58\,300\times$ and an accelerating voltage of 100 kV (LaB$_6$ illumination). The defocus was chosen in

all cases to be 1.2 μm corresponding to a first zero of the phase contrast transfer function at 2.1 nm.

X-ray crystal-structure determination: Intensity data were collected at 100 K on a Bruker-Nonius KappaCCD diffractometer using Mo$_{K\alpha}$ radiation ($\lambda = 0.71073$ Å, graphite monochromator). The structure was solved by direct methods and refined on F^2 using full-matrix least-squares procedures (SHELXTL NT 6.12). All non-hydrogen atoms were refined with anisotropic displacement parameters. Hydrogen atoms were placed in positions of optimized geometry; their isotropic displacement parameters were tied to those of their corresponding carrier atoms by a factor of 1.2 or 1.5. The least-squares refinement converged normally with residuals of $R_1 = 0.1236$, $wR_2 = 0.1556$, and GOF $= 1.031$ (all data). $C_{20}H_{35}NO_7$; monoclinic; space group $P2_1/c$; $a = 25.654(7)$, $b = 5.4720(8)$, $c = 15.649(2)$ Å; $\beta = 100.18(2)°$; $V = 2162.2(7)$ Å^3; $Z = 4$; $\rho_{calcd} = 1.233$ Mg m^{-3}; $F(000) = 872$; $R_1(F) = 0.0620$; $wR_2(F^2) = 0.1315$ ($I > 2\sigma(I)$). CCDC-775347 (**6**) contains the supplementary crystallographic data for this paper. These data can be obtained free of charge from The Cambridge Crystallographic Data Centre via www.ccdc.cam.ac.uk/data_request/cif.

Synthesis

General procedure I (GP I)—Acyl chloride esterification: Newkome dendrimer **14**[26] or **19**[28] (1 equiv) was dissolved in dry CH$_2$Cl$_2$ together with EtN$_3$ (1.5 equiv) and acyl chloride (1.5 equiv). The solution was stirred at room temperature for 24 h (TLC control) and then washed with 10% citric acid and NaCl solution before the organic phases were dried over MgSO$_4$. The products were purified by column chromatography.

General procedure II (GP II)—Cleavage of tert-*butyl esters*: Substances were dissolved in an excess amount of formic acid and stirred for 24 h at room temperature. The acid was then removed and the residue was precipitated several times from toluene.

Synthesis of compound 15: Amine-G1 **14** (1 g, 2.41 mmol) was converted using propanoyl chloride (252 μL, 2.89 mmol) by following GP I. The product was purified by column chromatography with cyclohexane/ethyl acetate (2:1) and was obtained as a white powder (749 mg, 1.59 mmol, 66%). ^{1}H NMR (300 MHz, CDCl$_3$, RT): $\delta = 1.09$ (t, $J = 7.5$ Hz, 3H; CH$_3$), 1.41 (s, 27H; CH$_3$), 1.94 (m, 6H; CH$_2$), 2.10 (q, $J = 7.5$ Hz, 2H; CH$_2$), 2.19 (m, 6H; CH$_2$), 5.77 ppm (s, 1H; NH); ^{13}C NMR (75.5 MHz, CDCl$_3$, RT): $\delta = 9.96$ (CH$_3$), 28.04 (CH$_3$), 29.77 (CH$_2$), 29.94 (CH$_2$), 30.48 (CH$_2$), 57.14 (C$_q$(NHR)), 80.64 (C$_q$(tBu)), 172.91 (C=O), 173.21 ppm (C=O); IR (ATR): $\tilde{\nu} = 2978, 1724, 1648, 1536, 1459, 1306, 1219, 1152, 1100, 848$ cm^{-1}; MS (MALDI-TOF, SIN): m/z: 471 $[M]^+$, 494 $[M+Na]^+$; elemental analysis calcd (%) for C$_{25}$H$_{45}$NO$_7$: C 63.67, H 9.62, N 2.97; found: C 63.37, H 9.41, N 2.96.

Synthesis of compound 4: Compound **15** (200 mg, 0.424 mmol) was treated by following GP II to yield the free acid. The product was obtained as a white powder (114 mg, 0.377 mmol, 89%). ^{1}H NMR (400 MHz, D$_2$O, RT): $\delta = 1.04$ (t, $J = 7.7$ Hz, 3H; CH$_3$), 1.95 (m, 6H; CH$_2$), 2.16 (q, $J = 7.7$ Hz, 2H; CH$_2$), 2.28 (m, 6H; CH$_2$), 3.67 ppm (s, 1H; NH); ^{13}C NMR (100.5 MHz, [D$_6$]DMSO, RT): $\delta = 10.29$ (CH$_3$), 28.09 (CH$_2$), 29.02 (CH$_2$), 29.11 (CH$_2$), 56.15 (C$_q$(NHR)), 172.91 (C=O), 174.55 ppm (C=O); IR (ATR): $\tilde{\nu} = 2937, 1702, 1654, 1556, 1375, 1320, 1284, 1222, 1105, 899$ cm^{-1}; MS (MALDI-TOF, DHB): m/z: 304 $[M+H]^+$, 326 $[M+Na]^+$; elemental analysis calcd (%) for C$_{13}$H$_{21}$NO$_7$: C 51.48, H 6.98, N 4.62; found: C 51.21, H 6.88, N 4.68.

Synthesis of compound 16: Amine-G1 **14** (1 g, 2.41 mmol) was reacted with hexanoyl chloride (400 μL, 2.89 mmol) by following GP I. The crude product was purified by column chromatography with cyclohexane/ethyl acetate (2:1) as eluent to isolate the product (815 mg, 1.59 mmol, 66%). ^{1}H NMR (300 MHz, CDCl$_3$, RT): $\delta = 0.87$ (t, $J = 6.5$ Hz, 3H; CH$_3$), 1.28 (m, 4H; CH$_2$), 1.41 (s, 27H; CH$_3$), 1.58 (q, $J = 6.5$ Hz, 2H; CH$_2$), 1.94 (m, 6H; CH$_2$), 2.07 (m, 2H; CH$_2$), 2.20 (m, 6H; CH$_2$), 5.77 ppm (s, 1H; NH); ^{13}C NMR (75.5 MHz, CDCl$_3$, RT): $\delta = 13.95$ (CH$_3$), 22.38 (CH$_2$), 25.47 (CH$_2$), 28.04 (CH$_3$), 29.78 (CH$_2$), 29.92 (CH$_2$), 31.42 (CH$_2$), 37.56 (CH$_2$), 57.23 (C$_q$(NHR)), 80.64 (C$_q$(tBu)), 172.59 (C=O), 172.91 ppm (C=O); IR (ATR): $\tilde{\nu} = 2938, 1717, 1675, 1531, 1366, 1319, 1210, 1150, 946, 845$ cm^{-1}; MS (MALDI-TOF, SIN): m/z: 514 $[M+H]^+$, 536 $[M+Na]^+$, 552 $[M+K]^+$; elemental analysis calcd (%) for C$_{28}$H$_{51}$NO$_7\cdot^1/_{12}$CDCl$_3$: C 64.40, H 9.85, N 2.67; found: C 64.62, H 9.76, N 2.65.

Synthesis of compound 5: Compound **16** (625 mg, 1.22 mmol) was treated by following GP II to yield the free acid (408 mg, 1.18 mmol, 97%). ^{1}H NMR (300 MHz, [D$_6$]DMSO, RT): $\delta = 0.85$ (t, $J = 6.5$ Hz, 3H; CH$_3$), 1.22 (m, 4H; CH$_2$), 1.45 (q, $J = 6.5$ Hz, 2H; CH$_2$), 1.82 (m, 6H; CH$_2$), 2.04 (m, 2H; CH$_2$), 2.07 (m, 6H; CH$_2$), 7.15 ppm (s, 1H; NH); ^{13}C NMR (75.5 MHz, [D$_6$]DMSO, RT): $\delta = 13.93$ (CH$_3$), 21.92 (CH$_2$), 25.18 (CH$_2$), 28.06 (CH$_2$), 28.97 (CH$_2$), 30.86 (CH$_2$), 35.83 (CH$_2$), 56.27 (C$_q$(NHR)), 172.09 (C=O), 174.51 ppm (C=O); IR (ATR): $\tilde{\nu} = 2930$, 1741, 1716, 1596, 1550, 1412, 1292, 1234, 1156, 850 cm^{-1}; MS (MALDI-TOF, SIN): m/z: 346 [M+H]$^+$, 368 [M+Na]$^+$; elemental analysis calcd (%) for C$_{16}$H$_{27}$NO$_7$: C 55.64, H 7.88, N 4.06; found: C 55.62, H 7.81, N 4.07.

Synthesis of compound 17: Amine-G1 (2 g, 4.82 mmol) was converted to **17** by reaction with decanoyl chloride (1.2 mL, 5.78 mmol) according to GP I. The crude product was purified by column chromatography with cyclohexane/ethyl acetate (2:1) as eluent to yield a white powder (860 mg, 1.51 mmol, 63%). ^{1}H NMR (300 MHz, CDCl$_3$, RT): $\delta = 0.84$ (t, $J = 6.5$ Hz, 3H; CH$_3$), 1.23 (m, 14H; CH$_2$), 1.40 (s, 27H; CH$_3$), 1.15 (q, $J = 6.5$ Hz, 2H; CH$_2$), 1.93 (m, 6H; CH$_2$), 2.06 (m, 2H; CH$_2$), 2.19 (m, 6H; CH$_2$), 5.76 ppm (s, 1H; NH); ^{13}C NMR (75.5 MHz, CDCl$_3$, RT): $\delta = 13.87$ (CH$_3$), 22.42 (CH$_2$), 25.52 (CH$_2$), 27.87 (CH$_3$), 29.05 (CH$_2$), 29.12 (CH$_2$), 29.21 (CH$_2$), 29.56 (CH$_2$), 29.71 (CH$_2$), 31.62 (CH$_2$), 37.38 (CH$_2$), 57.02 (C$_q$(NHR)), 80.40 (C$_q$(tBu)), 172.38 (C=O), 172.69 ppm (C=O); IR (ATR): $\tilde{\nu} = 2921$, 1724, 1674, 1532, 1458, 1365, 1320, 1218, 1151, 847 cm^{-1}; MS (MALDI-TOF, SIN): m/z: 593 [M+Na]$^+$, 609 [M+K]$^+$; elemental analysis calcd (%) for C$_{32}$H$_{59}$NO$_7$: C 67.45, H 10.44, N 2.46; found: C 67.70, H 10.31, N 2.26.

Synthesis of compound 6: Deprotection of the *tert*-butyl ester of **17** (706 mg, 1.51 mmol) led to product **6** (550 mg, 1.37 mmol, 91%) by following GP II. ^{1}H NMR (300 MHz, [D$_6$]DMSO, RT): $\delta = 0.83$ (t, $J = 6.5$ Hz, 3H; CH$_3$), 1.21 (m, 14H; CH$_2$), 1.42 (m, 2H; CH$_2$), 1.79 (m, 6H; CH$_2$), 2.05 (m, 2H; CH$_2$), 2.19 (m, 6H; CH$_2$), 7.15 ppm (s, 1H; NH); ^{13}C NMR (100.5 MHz, [D$_6$]DMSO, RT): $\delta = 14.14$ (CH$_3$), 22.26 (CH$_2$), 25.63 (CH$_2$), 28.22 (CH$_2$), 28.71 (CH$_2$), 28.82 (CH$_2$), 28.94 (CH$_2$), 29.08 (CH$_2$), 31.44 (CH$_2$), 36.01 (CH$_2$), 56.46 (C$_q$(NHR)), 172.47 (C=O), 174.71 ppm (C=O); IR (ATR): $\tilde{\nu} = 2916$, 1725, 1694, 1630, 1519, 1414, 1295, 1100, 921, 823 cm^{-1}; MS (MALDI-TOF, SIN): m/z: 402 [M+H]$^+$, 424 [M+Na]$^+$; elemental analysis calcd (%) for C$_{20}$H$_{35}$NO$_7$·^{1}/$_{18}$ C$_7$H$_8$: C 60.23, H 8.79, N 3.44; found: C 60.57, H 8.79, N 3.34.

Synthesis of compound 18:[38] Amine-G1 (1 g, 2.41 mmol) was treated with tetradecanoyl chloride (782 μL, 2.89 mmol) following GP I. The crude product was purified by column chromatography with cyclohexane/ethyl acetate (2:1) as eluent. A white powder was obtained (1.04 g, 1.66 mmol, 69%). ^{1}H NMR (300 MHz, CDCl$_3$, RT): $\delta = 0.85$ (t, $J = 6.5$ Hz, 3H; CH$_3$), 1.23 (m, 20H; CH$_2$), 1.41 (s, 27H; CH$_3$), 1.55 (q, $J = 6.5$ Hz, 2H; CH$_2$), 1.94 (m, 6H; CH$_2$), 2.07 (m, 2H; CH$_2$), 2.19 (m, 6H; CH$_2$), 5.76 ppm (s, 1H; NH); ^{13}C NMR (75.5 MHz, CDCl$_3$, RT): $\delta = 14.11$ (CH$_3$), 22.67 (CH$_2$), 25.80 (CH$_2$), 28.05 (CH$_3$), 29.34 (CH$_2$), 29.50 (CH$_2$), 29.63 (CH$_2$), 29.79 (CH$_2$), 29.93 (CH$_2$), 31.90 (CH$_2$), 37.61 (CH$_2$), 57.22 (C$_q$(NHR)), 80.63 (C$_q$(tBu)), 172.61 (C=O), 172.92 ppm (C=O); IR (ATR): $\tilde{\nu} = 2918$, 1720, 1677, 1538, 1457, 1367, 1315, 1148, 945, 848 cm^{-1}; MS (MALDI-TOF, DCTB): m/z: 649 [M+Na]$^+$, 665 [M+K]$^+$, 758 [M+Cs]$^+$; elemental analysis calcd (%) for C$_{36}$H$_{67}$NO$_7$: C 69.08, H 10.79, N 2.24; found: C 69.08, H 10.64, N 2.27.

Synthesis of compound 7:[38] Compound **18** (200 mg, 0.32 mmol) was treated following GP II to get the free acid (121 mg, 0.26 mmol, 82%). ^{1}H NMR (300 MHz, D$_2$O, RT): $\delta = 0.81$ (t, $J = 6.5$ Hz, 3H; CH$_3$), 1.21 (m, 20H; CH$_2$), 1.54 (q, $J = 6.5$ Hz, 2H; CH$_2$), 1.91 (m, 24H; CH$_2$), 2.18 (m, 24H; CH$_2$), 3.66 (s, 3H; NH); ^{13}C NMR (100.5 MHz, [D$_6$]DMSO, RT): $\delta = 13.97$ (CH$_3$), 22.10 (CH$_2$), 25.45 (CH$_2$), 28.03 (CH$_2$), 28.71 (CH$_2$), 28.78 (CH$_2$), 28.97 (CH$_2$), 29.03 (CH$_2$), 31.30 (CH$_2$), 56.23 (C$_q$(NHR)), 172.06 (C=O), 174.45 ppm (C=O); IR (ATR): $\tilde{\nu} = 2916$, 1723, 1694, 1635, 1520, 1412, 1295, 1175, 915, 822 cm^{-1}; MS (MALDI-TOF, SIN): m/z: 458 [M]$^+$; elemental analysis calcd (%) for C$_{24}$H$_{43}$NO$_7$: C 62.99, H 9.47, N 3.06; found: C 62.59, H 9.22, N 3.08.

Synthesis of compound 8: Deprotection of the *tert*-butyl ester[28] led to the free acid analogously following GP II. A white powder was isolated (423 mg, 0.309 mmol, 86%). ^{1}H NMR (300 MHz, [D$_6$]DMSO, RT): $\delta = 1.80$ (m, 24H; CH$_2$), 2.07 (m, 24H; CH$_2$), 7.32 ppm (s, 3H; NH);

^{13}C NMR (100.5 MHz, [D$_6$]DMSO, RT): $\delta = 28.20$ (CH$_2$), 29.15 (CH$_2$), 30.27 (CH$_2$), 31.26 (CH$_2$), 56.64 (C$_q$(NHR)), 93.47 (C$_q$(NO$_2$)), 170.76 (C=O), 174.69 ppm (C=O); IR (ATR): $\tilde{\nu} = 2945$, 1707, 1629, 1538, 1417, 1300, 1198, 1104, 911 cm^{-1}; elemental analysis calcd (%) for C$_{40}$H$_{60}$N$_4$O$_{23}$: C 49.79, H 6.27, N 5.81; found: C 49.76, H 6.51, N 5.69.

Synthesis of compound 20: Newkome amine-G2 **19** (500 mg, 0.348 mmol) was treated with propanoyl chloride (46 μL, 0.522 mmol) following GP I. The product was purified by column chromatography with cyclohexane/ethyl acetate (2:1) to yield a white powder (321 mg, 0.215 mmol, 62%). ^{1}H NMR (300 MHz, CDCl$_3$, RT): $\delta = 1.09$ (t, $J = 6.5$ Hz, 3H; CH$_3$), 1.41 (s, 81H; CH$_3$), 1.92 (m, 24H; CH$_2$), 2.15 (m, 24H; CH$_2$), 4.08 (q, 2H; CH$_2$), 6.04 (s, 3H; NH), 7.65 ppm (s, 1H; NH); ^{13}C NMR (75.5 MHz, CDCl$_3$, RT): $\delta = 28.48$ (CH$_3$), 30.19 (CH$_2$), 32.16 (CH$_2$), 32.43 (CH$_2$), 57.81 (C$_q$(NHR)), 80.99 (C$_q$(tBu)), 173.09 (C=O), 174.17 ppm (C=O); IR (ATR): $\tilde{\nu} = 2978$, 1730, 1653, 1539, 1368, 1317, 1253, 1216, 1152, 848 cm^{-1}; MS (MALDI-TOF, DHB): m/z: 1518 [M+Na]$^+$; elemental analysis calcd (%) for C$_{79}$H$_{138}$N$_4$O$_{22}$: C 63.43, H 9.30, N 3.75; found: C 63.09, H 9.18, N 3.74.

Synthesis of compound 9: *tert*-Butyl ester **20** (321 mg, 0.215 mmol) was treated following GP II to obtain the free acid (221 mg, 0.205 mmol, 95%). ^{1}H NMR (300 MHz, D$_2$O, RT): $\delta = 1.04$ (t, 3H; CH$_3$), 1.93 (m, 24H; CH$_2$), 2.18 (m, 26H; CH$_2$), 8.37 ppm (s, 3H; NH); ^{13}C NMR (100.5 MHz, [D$_6$]DMSO, RT): $\delta = 10.41$ (CH$_3$), 28.25 (CH$_2$), 29.19 (CH$_2$), 30.44 (CH$_2$), 56.52 (C$_q$(NHR)), 56.85 (C$_q$(NHR)), 172.64 (C=O), 173.19 (C=O), 174.73 ppm (C=O); IR (ATR): $\tilde{\nu} = 3331$, 2947, 1709, 1634, 1544, 1348, 1290, 1203, 1104, 910 cm^{-1}; MS (FAB, NBA): m/z: 991 [M]$^+$, 1013 [M+Na]$^+$; elemental analysis calcd (%) for C$_{43}$H$_{66}$N$_4$O$_{22}$·0.5 CDCl$_3$: C 49.70, H 6.42, N 5.33; found: C 50.01, H 6.74, N 5.35.

Synthesis of compound 21: Amine-G2 (250 mg, 0.174 mmol) was treated with hexanoyl chloride (36 μL, 0.261 mmol) following GP I. The crude product was purified by column chromatography with cyclohexane/ethyl acetate (2:1) as eluent. The product was obtained as a white powder (150 mg, 0.097 mmol, 56%). ^{1}H NMR (300 MHz, CDCl$_3$, RT): $\delta = 0.85$ (t, $J = 6.5$ Hz, 3H; CH$_3$), 1.23 (m, 8H; CH$_2$), 1.41 (s, 81H; CH$_3$), 1.92 (m, 24H; CH$_2$), 2.16 (m, 24H; CH$_2$), 6.01 (s, 3H; NH), 7.52 ppm (s, 1H; NH); ^{13}C NMR (100.5 MHz, CDCl$_3$, RT): $\delta = 14.01$ (CH$_3$), 22.35 (CH$_2$), 25.44 (CH$_2$), 28.08 (CH$_3$), 29.79 (CH$_2$), 29.85 (CH$_2$), 31.46 (CH$_2$), 31.80 (CH$_2$), 32.11 (CH$_2$), 37.40 (CH$_2$), 57.42 (C$_q$(NHR)), 80.58 (C$_q$(tBu)), 172.68 (C=O), 172.90 ppm (C=O); IR (ATR): $\tilde{\nu} = 2979$, 1727, 1680, 1536, 1367, 1318, 1253, 1152, 1104, 848 cm^{-1}; MS (FAB, NBA): m/z: 1539 [M]$^+$; elemental analysis calcd (%) for C$_{82}$H$_{144}$N$_4$O$_{22}$·0.5 CDCl$_3$: C 62.00, H 9.14, N 3.51; found: C 62.11, H 8.98, N 3.77.

Synthesis of compound 10: *tert*-Butyl ester **21** (150 mg, 0.097 mmol) was treated following GP II to get the free acid (96 mg, 0.093 mmol, 96%). ^{1}H NMR (300 MHz, D$_2$O, RT): $\delta = 0.81$ (t, 3H; CH$_3$), 1.23 (m, 4H; CH$_2$), 1.85 (m, 24H; CH$_2$), 2.11 (m, 28H; CH$_2$), 3.65 (s, 3H; NH), 8.39 ppm (s, 1H; NH); ^{13}C NMR (75.5 MHz, [D$_6$]DMSO, RT): $\delta = 14.05$ (CH$_3$), 22.35 (CH$_2$), 25.44 (CH$_2$), 29.79 (CH$_2$), 29.85 (CH$_2$), 31.46 (CH$_2$), 31.80 (CH$_2$), 32.11 (CH$_2$), 37.40 (CH$_2$), 56.49 (C$_q$(NHR)), 172.60 (C=O), 174.72 ppm (C=O); IR (ATR): $\tilde{\nu} = 2946$, 1706, 1539, 1413, 1293, 1197, 1102, 909, 832 cm^{-1}; MS (MALDI-TOF, DHB): m/z: 1032 [M]$^+$; elemental analysis calcd (%) for C$_{46}$H$_{72}$N$_4$O$_{22}$·1.5 CDCl$_3$: C 47.01, H 6.23, N 4.62; found: C 47.10, H 6.38, N 5.28.

Synthesis of compound 22: Amine-G2 (500 mg, 0.348 mmol) was treated with decanoyl chloride (563 μL, 0.522 mmol) according to GP I. The crude product was purified by column chromatography with cyclohexane/ethyl acetate (2:1) as eluent. The product was isolated as a white powder (431 mg, 0.270 mmol, 78%). ^{1}H NMR (300 MHz, CDCl$_3$, RT): $\delta = 0.85$ (t, $J = 6.5$ Hz, 3H; CH$_3$), 1.23 (m, 16H; CH$_2$), 1.41 (s, 81H; CH$_3$), 1.92 (m, 24H; CH$_2$), 2.16 (m, 24H; CH$_2$), 6.01 (s, 3H; NH), 7.52 ppm (s, 1H; NH); ^{13}C NMR (100.5 MHz, CDCl$_3$, RT): $\delta = 14.10$ (CH$_3$), 22.66 (CH2), 28.07 (CH$_3$), 29.31 (CH$_2$), 29.52 (CH$_2$), 29.78 (CH$_2$), 29.82 (CH$_2$), 31.85 (CH$_2$), 32.07 (CH$_2$), 57.41 (C$_q$(NHR)), 80.56 (C$_q$(tBu)), 172.66 (C=O), 172.86 ppm (C=O); IR (ATR): $\tilde{\nu} = 2932$, 1728, 1653, 1539, 1457, 1367, 1315, 1253, 1151, 849 cm^{-1}; MS (FAB, NBA): m/z: 1595 [M]$^+$; elemental analysis calcd (%) for C$_{86}$H$_{152}$N$_4$O$_{22}$: C 64.79, H 9.61, N 3.51; found: C 64.67, H 9.50, N 3.53.

Synthesis of compound 11: Deprotection of the *tert*-butyl ester of **22** led to compound **11** (253 mg, 0.232 mmol, 86%) following GP II. ^{1}H NMR (300 MHz, D$_2$O, RT): $\delta = 0.80$ (t, 3H; CH$_3$), 1.22 (m, 14H; CH$_2$), 1.53 (m, 2H; CH$_2$), 1.90 (m, 24H; CH$_2$), 2.15 (m, 24H; CH$_2$), 3.66 (s, 3H; NH), 8.34 ppm (s, 1H; NH); ^{13}C NMR (100.5 MHz, [D$_6$]DMSO, RT): $\delta = 13.99$ (CH$_3$), 21.06 (CH$_2$), 25.47 (CH$_2$), 28.06 (CH$_2$), 28.74 (CH$_2$), 28.81 (CH$_2$), 28.95 (CH$_2$), 29.05 (CH$_2$), 30.20 (CH$_2$), 30.67 (CH$_2$), 31.29 (CH$_2$), 56.24 (C$_q$(NHR)), 56.70 (C$_q$(NHR)), 171.95 (C=O), 172.24 (C=O), 174.46 ppm (C=O); IR (ATR): $\tilde{\nu} = 2930$, 1717, 1543, 1417, 1368, 1305, 1217, 1156, 916, 847 cm^{-1}; MS (FAB, NBA): *m/z*: 1090 [*M*]$^+$; elemental analysis calcd (%) for C$_{50}$H$_{80}$N$_4$O$_{22}$: C 55.18, H 7.40, N 5.14; found: C 54.83, H 7.35, N 4.98.

Synthesis of compound 23: Amine-G2 (250 mg, 0.174 mmol) was treated with tetradecanoyl chloride (70 µL, 0.261 mmol) following GP I. The crude product was purified by column chromatography with cyclohexane/ethyl acetate (2:1) as eluent to obtain a white powder (59 mg, 0.09 mmol, 54%). ^{1}H NMR (300 MHz, CDCl$_3$, RT): $\delta = 0.86$ (t, *J* = 6.8 Hz, 3H; CH$_3$), 1.23 (m, 24H; CH$_2$), 1.41 (s, 81H; CH$_3$), 1.95 (m, 24H; CH$_2$), 2.18 (m, 24H; CH$_2$), 6.07 (s, 3H; NH), 7.61 ppm (s, 1H; NH); ^{13}C NMR (100.5 MHz, CDCl$_3$, RT): $\delta = 14.11$ (CH$_3$), 22.67 (CH2), 28.08 (CH$_3$), 29.35 (CH$_2$), 29.43 (CH$_2$), 29.66 (CH$_2$), 29.78 (CH$_2$), 29.84 (CH$_2$), 31.78 (CH$_2$), 31.91 (CH$_2$), 32.07 (CH$_2$), 57.44 (C$_q$(NHR)), 80.56 (C$_q$(*t*Bu)), 172.68 (C=O), 172.91 ppm (C=O); IR (ATR): $\tilde{\nu} = 2930$, 1729, 1654, 1539, 1457, 1367, 1316, 1255, 1151, 849 cm^{-1}; MS (FAB, NBA): *m/z*: 1650 [*M*]$^+$, 1672 [*M*+Na]$^+$; elemental analysis calcd (%) for C$_{90}$H$_{160}$N$_4$O$_{22}$: C 65.50, H 9.77, N 3.40; found: C 65.33, H 9.62, N 3.19.

Synthesis of compound 12: Compound **12** was obtained through cleavage of the *tert*-butyl ester of **23** following GP II in a yield of 102 mg (0.08 mmol, 96%). ^{1}H NMR (300 MHz, D$_2$O, RT): $\delta = 0.81$ (t, 3H; CH$_3$), 1.21 (m, 20H; CH$_2$), 1.54 (m, 2H; CH$_2$), 1.91 (m, 24H; CH$_2$), 2.18 (m, 24H; CH$_2$), 3.66 (s, 3H; NH), 8.39 ppm (s, 1H; NH); ^{13}C NMR (100.5 MHz, [D$_6$]DMSO, RT): $\delta = 13.98$ (CH$_3$), 18.19 (CH$_2$), 22.11 (CH$_2$), 25.48 (CH$_2$), 28.07 (CH$_2$), 28.74 (CH$_2$), 28.77 (CH$_2$), 28.84 (CH$_2$), 28.91 (CH$_2$), 29.05 (CH$_2$), 29.11 (CH$_2$), 30.20 (CH$_2$), 30.67 (CH$_2$), 31.32 (CH$_2$), 36.17 (CH$_2$), 56.25 (C$_q$(NHR)), 56.70 (C$_q$(NHR)), 171.95 (C=O), 172.25 (C=O), 174.47 ppm (C=O); IR (ATR): $\tilde{\nu} = 2926$, 2853, 1707, 1544, 1458, 1414, 1289, 1214, 1104, 915 cm^{-1}; MS (FAB, NBA): *m/z*: 1145 [*M*]$^+$, 1167 [*M*+Na]$^+$; elemental analysis calcd (%) for C$_{54}$H$_{88}$N$_4$O$_{22}$: C 56.63, H 7.74, N 4.89; found: C 56.42, H 7.79, N 4.62.

Synthesis of compound 24: Triacontanoic acid (250 mg, 0.552 mmol) was dissolved in dry DMF (40 mL) together with DCC (1.5 equiv; 215 mg, 1.04 mmol) and HOBt (3.5 equiv; 141 mg, 1.04 mmol) and was stirred for 1 h at 0°C. Then amine (794 mg, 0.552 mmol) was added to the solution and the mixture was stirred for about 2.5 d at RT (TLC control). The white precipitate was filtered off and the DMF was removed before the residue was dissolved in chloroform and washed with 10% citric acid solution, NaHCO$_3$ solution, and NaCl solution. The organic phases were dried over MgSO$_4$. The product was purified by column chromatography with cyclohexane/ethyl acetate (2:1) to yield a white powder (672 mg, 0.359 mmol, 65%). ^{1}H NMR (300 MHz, CDCl$_3$, RT): $\delta = 0.85$ (t, *J* = 7.2 Hz, 3H; CH$_3$), 1.22 (m, 56H; CH$_2$), 1.40 (s, 81H; CH$_3$), 1.92 (m, 24H; CH$_2$), 2.14 (m, 24H; CH$_2$), 6.01 (s, 3H; NH), 7.52 ppm (s, 1H; NH); ^{13}C NMR (100.5 MHz, CDCl$_3$, RT): $\delta = 14.12$ (CH$_3$), 22.68 (CH$_2$), 25.82 (CH$_2$), 26.88 (12C; CH$_2$), 28.06 (27C; CH$_3$), 29.35 (2C; CH$_2$), 29.45 (2C; CH$_2$), 29.64 (4C; CH$_2$), 29.68 (12C; CH$_2$), 29.74 (12C; CH$_2$), 31.75 (2C, CH$_2$), 31.90 (2C; CH$_2$), 32.01 (CH$_2$), 37.49 (CH$_2$), 57.38 (C$_q$(NHR)), 172.65 (C=O), 172.85 (C=O), 173.67 ppm (C=O); IR (ATR): $\tilde{\nu} = 2923$, 2853, 1728, 1538, 1456, 1366, 1313, 1253, 1147, 848 cm^{-1}; MS (FAB, NBA): *m/z*: 1872 [*M*]$^+$, 1895 [*M*+Na]$^+$; elemental analysis calcd (%) for C$_{106}$H$_{192}$N$_4$O$_{22}$·0.5 CDCl$_3$: C 66.11, H 10.05, N 2.90; found: C 66.07, H 10.08, N 3.27.

Synthesis of compound 13: Cleavage of the *tert*-butyl ester of compound **24** led to product **13** following GP II. Yield: 423 mg (0.309 mmol, 86%). ^{1}H NMR (300 MHz, D$_2$O, RT): $\delta = 0.84$ (t, *J* = 7.2 Hz, 3H; CH$_3$), 1.23 (m, 56H; CH$_2$), 1.91 (m, 24H; CH$_2$), 2.16 (m, 24H; CH$_2$), 6.31 (s, 3H; NH), 7.42 ppm (s, 1H; NH); ^{13}C NMR (100.5 MHz, [D$_6$]DMSO, RT): $\delta = 13.98$ (CH$_3$), 21.98 (CH$_2$), 22.12 (4C; CH$_2$), 25.50 (CH$_2$), 28.06 (12C; CH$_2$), 28.73 (4C; CH$_2$), 28.81 (3C; CH$_2$), 28.89 (4C; CH$_2$), 29.01 (12C; CH$_2$),

30.20 (2C; CH$_2$), 30.67 (CH$_2$), 30.82 (CH$_2$), 31.31 (4C; CH$_2$), 35.81 (CH$_2$), 36.17 (CH$_2$), 56.24 (C$_q$(NHR)), 56.70 (C$_q$(NHR)), 171.95 (C=O), 172.25 (C=O), 174.47 ppm (C=O); IR (ATR): $\tilde{\nu} = 2921$, 2852, 1710, 1544, 1460, 1367, 1291, 1251, 1103, 910 cm^{-1}; MS (FAB, NBA): *m/z*: 1369 [*M*]$^+$, 1391 [*M*+Na]$^+$; elemental analysis calcd (%) for C$_{70}$H$_{120}$N$_4$O$_{22}$·0.5[D$_6$]DMSO: C 60.40, H 9.00, N 3.97; found: C 60.70, H 9.04, N 4.04.

MD simulation protocol: Two fully deprotonated monomeric dendrimer amphiphiles **1** were initially placed in a "head-to-head" orientation to each other. Care was taken to avoid clashes between the monomers. Thirty six Na, K, or Li counterions were then put in place using the program *leap* from the Amber suite of programs. The system was placed in a truncated octahedral SPC/E explicit water[39] box with at least 15 Å between the solute and the box borders. The box size was chosen to allow dissociation of the monomers. The force-field parameters for the amphiphiles were taken from the general Amber force field (GAFF)[40] used in our previous publications.[25, 32] The ion parameters were taken from Joung and Cheatham,[41] and are especially designed to account for proper representations of ion effects in combination with the chosen water model. After solvating the system, additional metal cations and chloride ions were added to give a final concentration of 0.1 M.

All simulations were carried out using Amber 10.[42] Periodic boundary conditions and constant pressure dynamics with isotropic position scaling at 300 K were used. The electrostatic interactions were treated using the particle mesh Ewald (PME) method[43] together with a cutoff for all non-bonded interactions of 8 Å. The order of the B-spline interpolation for PME was 4, which implies a cubic spline approximation. The width of the nonbonded skin was 2.0 Å.

The system was minimized by 5000 steps of steepest descent minimization followed by a full conjugate gradient minimization. Subsequently, the systems were equilibrated and heated to the target temperature of 300 K. The integration time step was 1 fs. During the equilibration phase, weak positional restraints were removed in a stepwise manner. During the first 500 ps, all heavy atoms of the monomers, except the hydrophobic chains, were held fixed. In the second equilibration phase (500 ps) only the nitrogen and oxygen atoms were kept rigid. The equilibration phase was followed by the production phase of the simulation.

Acknowledgements

[1] M. Kellermann, W. Bauer, A. Hirsch, B. Schade, K. Ludwig, C. Böttcher, *Angew. Chem.* **2004**, *116*, 3019–3022; *Angew. Chem. Int. Ed.* **2004**, *43*, 2959–2962.

[2] S. Burghardt, A. Hirsch, B. Schade, K. Ludwig, C. Böttcher, *Angew. Chem.* **2005**, *117*, 3036–3039; *Angew. Chem. Int. Ed.* **2005**, *44*, 2976–2979.

[3] B. Schade, K. Ludwig, C. Böttcher, U. Hartnagel, A. Hirsch, *Angew. Chem.* **2007**, *119*, 4472–4475; *Angew. Chem. Int. Ed.* **2007**, *46*, 4393–4396.

[4] M. Brettreich, S. Burghardt, C. Böttcher, T. Bayerl, S. Bayerl, A. Hirsch, *Angew. Chem.* **2000**, *112*, 1915–1918; *Angew. Chem. Int. Ed.* **2000**, *39*, 1845–1848.

[5] W. Kunz, J. Henle, B. W. Ninham, *Curr. Opin. Colloid Interface Sci.* **2004**, *9*, 19–37.

[6] Y. Zhang, P. S. Cremer, *Curr. Opin. Chem. Biol.* **2006**, *10*, 658–663.

[7] M. C. Pinna, P. Bauduin, D. Touraud, M. Monduzzi, B. W. Ninham, W. Kunz, *J. Phys. Chem. B* **2005**, *109*, 16511–16514.

[8] M. C. Pinna, A. Salis, M. Monduzzi, W. Ninham Barry, *J. Phys. Chem. B* **2005**, *109*, 5406–5408.

[9] L. Vrbka, P. Jungwirth, P. Bauduin, D. Touraud, W. Kunz, *J. Phys. Chem. B* **2006**, *110*, 7036–7043.

CHEMISTRY
A EUROPEAN JOURNAL

[10] J. M. Broering, A. S. Bommarius, *J. Phys. Chem. B* **2005**, *109*, 20612–20619.

[11] R. Perez-Jimenez, R. Godoy-Ruiz, B. Ibarra-Molero, J. M. Sanchez-Ruiz, *Biophys. J.* **2004**, *86*, 2414–2429.

[12] R. A. Curtis, L. Lue, *Chem. Eng. Sci.* **2005**, *60-60*, 907–923.

[13] K. D. Collins, G. W. Neilson, J. E. Enderby, *Biophys. Chem.* **2007**, *128*, 95–104.

[14] R. Vacha, S. W. I. Siu, M. Petrov, R. A. Bockmann, J. Barucha-Kraszewska, P. Jurkiewicz, M. Hof, M. L. Berkowitz, P. Jungwirth, *J. Phys. Chem. A* **2009**, *113*, 7235–7243.

[15] J. Heyda, J. Pokorna, L. Vrbka, R. Vacha, B. Jagoda-Cwiklik, J. Konvalinka, P. Jungwirth, J. Vondrasek, *PCH PhysicoChem. Hydrodyn.* **2009**, *11*, 7599–7604.

[16] W. Kunz, P. Lo Nostro, B. W. Ninham, *Curr. Opin. Colloid Interface Sci.* **2004**, *9*, 1–18.

[17] A. Hirsch, *Pure Appl. Chem.* **2008**, *80*, 571–587.

[18] M. Becherer, B. Schade, C. Böttcher, A. Hirsch, *Chem. Eur. J.* **2009**, *15*, 1637–1648.

[19] C. D. Schmidt, C. Böttcher, A. Hirsch, *Eur. J. Org. Chem.* **2007**, 5497–5505.

[20] C. D. Schmidt, C. Böttcher, A. Hirsch, *Eur. J. Org. Chem.* **2009**, 5337–5349.

[21] C. Backes, C. D. Schmidt, F. Hauke, C. Böttcher, A. Hirsch, *J. Am. Chem. Soc.* **2009**, *131*, 2172–2184.

[22] C. Backes, F. Hauke, C. D. Schmidt, A. Hirsch, *Chem. Commun.* **2009**, 2643–2645.

[23] C. Ehli, C. Oelsner, D. M. Guldi, A. Mateo-Alonso, M. Prato, C. Schmidt, C. Backes, F. Hauke, A. Hirsch, *Nat. Chem. Biol.* **2009**, *1*, 243–249.

[24] J. M. Englert, J. Röhrl, C. D. Schmidt, R. Graupner, M. Hundhausen, F. Hauke, A. Hirsch, *Adv. Mater.* **2009**, *21*, 4265–4269.

[25] C. M. Jäger, A. Hirsch, B. Schade, K. Ludwig, C. Böttcher, T. Clark, *Langmuir* **2010**, *26*, 10460–10466.

[26] G. R. Newkome, R. K. Behera, C. N. Moorefield, G. R. Baker, *J. Org. Chem.* **1991**, *56*, 7162–7167.

[27] G. R. Newkome, A. Nayak, R. K. Behera, C. N. Moorefield, G. R. Baker, *J. Org. Chem.* **1992**, *57*, 358–362.

[28] M. Brettreich, A. Hirsch, *Synlett* **1998**, 1396–1398.

[29] J. Haldar, V. K. Aswal, P. S. Goyal, S. Bhattacharya, *Angew. Chem.* **2001**, *113*, 1278–1282; *Angew. Chem. Int. Ed.* **2001**, *40*, 1228–1232.

[30] A. Patist, S. G. Oh, R. Leung, D. O. Shah, *Colloids Surf. A* **2001**, *176*, 3–16.

[31] J. R. Bellare, T. Kaneko, D. F. Evans, *Langmuir* **1988**, *4*, 1066–1067.

[32] C. M. Jäger, A. Hirsch, B. Schade, C. Böttcher, T. Clark, *Chem. Eur. J.* **2009**, *15*, 8586–8592.

[33] K. D. Collins, *Methods* **2004**, *34*, 300–311.

[34] K. D. Collins, *Biophys. J.* **1997**, *72*, 65–76.

[35] K. D. Collins, *Biophys. Chem.* **2006**, *119*, 271–281.

[36] C. J. Carrell, H. L. Carrell, J. Erlebacher, J. P. Glusker, *J. Am. Chem. Soc.* **1988**, *110*, 8651–8656.

[37] B. Hess, N. F. van der Vegt, *Proc. Natl. Acad. Sci. USA* **2009**, *106*, 13296–13300.

[38] A. A. Williams, B. S. Day, B. L. Kite, M. K. McPherson, C. Slebodnick, J. R. Morris, R. D. Gandour, *Chem. Commun.* **2005**, 5053–5055.

[39] H. J. C. Berendsen, J. R. Grigera, T. P. Straatsma, *J. Phys. Chem.* **1987**, *91*, 6269–6271.

[40] J. Wang, R. M. Wolf, J. W. Caldwell, P. A. Kollman, D. A. Case, *J. Comput. Chem.* **2004**, *25*, 1157–1174.

[41] I. S. Joung, T. E. Cheatham, *J. Phys. Chem. B* **2008**, *112*, 9020–9041.

[42] AMBER 10, D. A. Case, T. A. Darden, I. Cheatham, Thomas E., C. L. Simmerling, J. Wang, R. E. Duke, R. Luo, M. Crowley, R. C. Walker, W. Zhang, K. M. Merz, B. Wang, S. Hayik, A. Roitberg, G. Seabra, I. Kolossvary, K. F. Wong, F. Paesani, J. Vanicek, X. Wu, S. R. Brozell, T. Steinbrecher, H. Gohlke, L. Yang, C. Tan, J. Mongan, V. Homak, G. Cui, D. H. Mathews, M. G. Seetin, C. Sagui, V. Babin, P. A. Kollman, **2008**, University of California, San Francisco.

[43] T. Darden, D. York, L. Pedersen, *J. Chem. Phys.* **1993**, *98*, 10089–10092.